Kinetics and Catalysis, Vol. 46, No. 1, 2005, pp. 10–20. Translated from Kinetika i Kataliz, Vol. 46, No. 1, 2005, pp. 14–25.

Configuration of the Chain Ignition Region and Dynamic Regimes of Methane Oxidation

A. A. Karnaukh and A. N. Ivanova

Institute of Chemical Physics, Russian Academy of Sciences, Chernogolovka, Moscow oblast, 142432 Russia

Received July 16, 2003

Abstract—The kinetics of the initial step of methane oxidation in a wide range of the external parameters is studied using a simplified model including complete branched cycles of peroxide formation and decomposition. An analytical formula for the ignition criterion is obtained by analysis of the structure of the reaction scheme (graph). Qualitative assessment and calculation of the critical parameters of this criterion in the framework of a linear model provide a new notion of the configuration of the methane chain ignition region. This notion implies that the kinetics and product composition vary in going from one portion of the ignition region boundary to another and provides an explanation for this behavior. The evolution of the system in the region itself is discussed in terms of nonlinear contributions to the dependence of the criterion on the parameters.

A deeper insight into the kinetics and mechanism of the oxidation of methane, which is the simplest and most abundant combustible material in nature and technogenic media, could contribute significantly to the development of a general theory of combustible systems. A large body of experimental and theoretical data has been accumulated in solving related problems. It makes it possible to interpret the rich phenomenology of hydrocarbon oxidation and combustion. The key oxidation steps, both linear and nonlinear, have been understood well to date. A special role in the progress in this field was played by the classical works by Lewis and von Elbe [1] and Shtern [2], who studied the phenomenology of hydrocarbon oxidation and combustion, and the fundamental kinetic ideas of Semenov [3], which were developed by his followers (see, e.g., [4–6] and references cited therein). Subsequent studies in this area pointed out the role of those elements of the mechanism which are common to methane and other hydrocarbons and are significant at low temperatures in the initial oxidation step [7–9]. The kinetics of the initial step is interesting, because it is believed to determine, to a considerable extent, the dynamics of the subsequent steps and the primary sources of heat and products.

The purpose of this work is to obtain an analytical expression for the ignition criterion for low-temperature methane oxidation, to see have the ignition limits vary over wide ranges of the parameters of the system, and to predict and interpret possible dynamic regimes of the process based on the data obtained. This work is expected to contribute to the notion of spontaneous ignition occurring under natural conditions (at pressures of about 1 atm) and, in some specially indicated cases, under more severe conditions.

CALCULATION PROCEDURE

The essence of the approach proposed in [10] for studying different critical phenomena in complex chemical systems is that the specific features of the interactions involved in the reaction network are related to the properties of the characteristic polynomial of the Jacobian matrix of the kinetic system. The roots of this polynomial (eigenvalues of the Jacobian matrix) determine the coefficients in the exponents of the time exponentials representing the solution of the set of kinetic equations within the linear approximation and, therefore, the qualitative type of process dynamics (for instance, the process rate grows exponentially if the coefficient is positive, the process is stable if all coefficients are negative, an oscillation regime develops if the roots are complex, and so on). Generally speaking, these are local characteristics of the system. However, under certain conditions, some global results concerning the dynamics of the process can be obtained. It is important that expressing the coefficients of the characteristic polynomial in terms of reaction rate constants and reactant concentrations be formalized to obtain formulas for critical conditions in analytical form (a FORTRAN 5 PC program has been written for deriving these formulas). This approach is presented in [11] as applied to ignition conditions, with examples of its use. The ignition condition, which we attribute to the maximum eigenvalue of the Jacobian matrix passing through zero, is the direct generalization of the Semenov criterion for complex systems. It coincides with the vanishing condition for the smallest coefficient of the characteristic polynomial. The contributions from so-called critical fragments to any coefficient of the characteristic polynomial are negative and are separated into a polynomial **A**, and the other contributions are positive and summed in a polynomial **B**. The criterion is presented in the form $\varphi = \mathbf{A} - \mathbf{B}$, and the ignition

0023-1584/05/4601-0010 © 2005 MAIK "Nauka/Interperiodica"

Table 1. Reactions linear with respect to the active centers in the low-temperature methane oxidation network[1]

Reaction[2]		A, $cm^3\ mol^{-1}\ s^{-1}$	n	E_a, kcal/mol	$-\Delta H$, kcal/mol	Notes[3]
$CH_4 + O_2 \longrightarrow CH_3^{\bullet} + HO_2^{\bullet}$	(0)	0.6×10^{14}	–	56/46[het4]	55.3	[17]/[8]
$CH_3^{\bullet} + O_2 + [M] \longrightarrow CH_3O_2^{\bullet} + [M]$	(I)	0.6×10^{26}	–3.3	0	–31.3	k^0 [18], K_{12}
$CH_3O_2^{\bullet} + [M] \longrightarrow CH_3^{\bullet} + O_2 + [M]$	(II)	0.9×10^{14}	–	31.3	31.3	[19], **IB**
$CH_3O_2^{\bullet} + CH_4 \longrightarrow CH_3^{\bullet} + CH_3OOH$	(III)	0.6×10^{12}	–	21.5	19	[17]
$HO_2^{\bullet} + CH_4 \longrightarrow CH_3^{\bullet} + H_2O_2$	(IV)	0.2×10^{13}	–	21.5	17.8	″
$CH_3OOH + [M] \longrightarrow CH_3O^{\bullet} + OH^{\bullet} + [M]$	(V)	0.16×10^{19}	–	39.7[5]	43.8	k^0, **IB**
$OH^{\bullet} + CH_4 \longrightarrow CH_3^{\bullet} + [H_2O]$	(VI)	0.8×10^{7}	1.92	2.67	–14.43	[17]
$CH_3O^{\bullet} + CH_4 \longrightarrow CH_3^{\bullet} + [CH_3OH]$	(VII)	0.6×10^{12}	–	11	1.65	″
$CH_3O^{\bullet} + O_2 \longrightarrow HO_2^{\bullet} + [CH_2O]$	(VIII)	0.6×10^{11}	–	2.61	–26.6	″
$H_2O_2 + [M] \longrightarrow 2OH^{\bullet} + [M]$	(IX)	0.12×10^{18}	–	45.5	51.3	k [18], **IB**
$H_2O_2 \longrightarrow$ wall $\longrightarrow$ decay	(X)	–	–	0	–	comb., **IA**
$CH_3O_2^{\bullet} \longrightarrow$ wall $\longrightarrow$ decay	(XI)	–	–	0	–	diff., **IA**
$HO_2^{\bullet} \longrightarrow$ wall $\longrightarrow$ decay	(XII)	–	–	0	–	″
$CH_3^{\bullet} \longrightarrow$ wall $\longrightarrow$ decay	(XIII)	–	–	0	–	″
$CH_3OOH \longrightarrow$ wall $\longrightarrow$ decay	(XIV)	–	–	0	–	comb., **IA**
$OH^{\bullet} + O_2 \longrightarrow HO_3^{\bullet}$	(XV)	0.35×10^{12}	–	1.2	–10(?)[6]	Analogue of $OH^{\bullet} + C_2H_4$ ([20]; see text)
$HO_3^{\bullet} \longrightarrow OH^{\bullet} + O_2$	(XVI)	10^{15}	–	25–28	–	
$HO_3^{\bullet} + [M] \longrightarrow$ decay	(XVII)	10^{12}	–	–	–	

[1] $k = AT^n \exp(-E_a/RT)$.

[2] Species that do not react in the framework of this linear model are given in brackets.

[3] k^0 are the constant values in the low-pressure limit; for **IA** and **IB**, see Appendix; diff. and comb. designate the diffusion and combined constants.

[4] Heterogeneous chain initiation.

[5] The calculation of E_a is based on data from [21].

[6] Estimated value.

region is defined by $\varphi > 0$. Note that branched cycles in the reaction network are always critical. This procedure was used to establish ignition limits for the oxidation of hydrogen [12], methane [13–15], and methane halides [16].

MODEL OF THE REACTION

Of the reactions involved in the oxidation model, the reactions responsible for the entry of the system into the chain ignition region are presented in Table 1. Most of these reactions and relevant constants are taken from the scheme used in our earlier works [7, 17] for nonisothermal simulation of the initial step of the two-step ignition of methane–air mixtures. Those works were devoted to so-called Melvin delays [22] at high pressures and moderate temperatures and to the mechanism of slow oxidation at pressures of ~1 atm. The network consisting of the reactions presented in Table 1 is the

Table 2. Reactions nonlinear with respect to the active centers in the low-temperature methane oxidation network[1]

Reaction		A, $cm^3\ mol^{-1}\ s^{-1}$	n	E_a, kcal/mol	$-\Delta H$, kcal/mol	Notes
$2CH_3^{\bullet} + [M] \longrightarrow [C_2H_6] + [M]$	(I')	0.13×10^{42}	–7	2.76	–89.8	k^0 [18], **IB**
$2CH_3O_2^{\bullet} \longrightarrow O_2 + [CH_3OH] + CH_2O$	(III')	0.22×10^{10}	–	1.5	–79.6	″
$2HO_2^{\bullet} \longrightarrow H_2O_2 + O_2$	(IV')	0.133×10^{12}	–	–1.63	–37.5	Sum of constants [18][2]
		0.42×10^{15}	–	12		
$HO_2^{\bullet} + CH_3O_2^{\bullet} \longrightarrow CH_3OOH + O_2$	(XVIII)	0.12×10^{12}	–	–1.57	–36.6	[17]
$CH_3O_2^{\bullet} + CH_2O \longrightarrow CH_3OOH + [HCO^{\bullet}]$	(XIX)	0.28×10^{12}	–	12	1.91	″
$2CH_3O_2^{\bullet} \longrightarrow 2CH_3O^{\bullet} + O_2$	(XX)	0.55×10^{11}	–	–0.84	0.62	″

[1] See notes to Table 1.

[2] The second term, $k_{4'}$, is recommended for the temperature range 850–1250 K.

modification tuned to 1 atm, and we use it mainly to establish the chain ignition limits. Accordingly, it does not include the reactions of intermediates that appear in the bulk of the system or on the wall and do not affect the ignition limit. Several reactions, whose existence and role have never been discussed in the literature on oxidation, are introduced in this model. These reactions describe the reversible association of $OH^{\bullet}$ radicals with oxygen (reactions (XV)–(XVII)). Reaction (XV), as well as the interaction of oxygen with a $CH_3O^{\bullet}$ radical (reaction (VII)), is sensitive to the proportions of the reactants and, hence, essential for the determination of the ignition limits as a function of mixture composition. The comparative stability of $HO_3^{\bullet}$ is confirmed by the relationship between the enthalpy of formation of $HO_x^{\bullet}$ species and the hyperfine interaction constant in their ESR spectra [23]. It turned out that both parameters are minimal at $x = 3$ ($-\Delta H_{HO_3^{\bullet}} \sim \pm 1$ kcal/mol [24]). The constants we list for the formation of the $HO_3^{\bullet}$ radical (reaction (XV)) and for the decomposition and deactivation of these radicals (reactions (XVI) and (XVII)) are close to the constants determined in [20] for the attachment of an $OH^{\bullet}$ radical to C_2H_4.

The nonlinear reactions between formaldehyde and the radicals whose decay is taken into account in Table 1 are presented in Table 2. All reactions in Table 2 starting at reaction (III') are positive interactions to an extent to which their products are reactive and can contribute noticeably to chain propagation. A necessary condition for chain propagation is the irreversible conversion of the methyl radical to the peroxy radical. This conversion is possible either at a rather low temperature and a high pressure or in excess oxygen. Otherwise, methyl radicals would rather recombine into ethane by reaction (I') to cause a considerable heating of the system and, eventually, radical decay.

LINEAR CRITERION

The ignition criterion corresponding to the reaction network presented in Table 1, under the assumption of constant concentrations of the starting reactants, has the form

$$\mathbf{A}_0 = \mathbf{B}_0, \tag{1}$$

where, after division by the common multiplier,

$$\mathbf{A}_0 = a\left(\frac{2}{1+l} + \frac{1}{(1+1/l)}\left(\frac{2+2/mL}{1+r} + \frac{1}{L(1+1/r)}\right)\right),$$

$$\mathbf{B}_0 = s(1+Q), \quad \alpha = \frac{[CH_4]}{[O_2]}, \quad a = \frac{k_3[CH_4]}{k_{11}},$$

$$b = \frac{k_2[M]}{k_{11}}, \quad l = \frac{k_8}{k_7\alpha}, \quad m = \left(1 + \frac{k_{10}}{k_9[M]}\right),$$

$$L = (1 + L_1/\alpha), \quad L_1 = \frac{k_{15}}{k_6(1 + k_{16}/k_{17}[M])},$$

$$Q = q(1 + a + b), \quad q = \frac{k_{13}}{k_1[M][O_2]}, \quad s = (1 + \tilde{s}),$$

$$\tilde{s} = \frac{k_{14}}{k_5[M]}, \quad r = \frac{k_{12}}{k_4[CH_4]}.$$

The dependences of $\mathbf{A}_0$ and $\mathbf{B}_0$ on the combinations of the starting parameters introduced are defined by the sums of linear fractional terms, including decreasing and increasing functions of these parameters. This fact is the reason for the nonmonotonic dependence of the criterion on the starting parameters, including mixture composition, pressure, and temperature. For example, the nonmonotonic temperature dependence is the reason for the phenomenon known as the negative temperature factor (NTF) of rate. The nature of this phenomenon is analyzed below. Considering that an increase in $\mathbf{A}_0$ or $\mathbf{B}_0$ reflects an increase in the accelerating and inhibiting factors, respectively, one can qualitatively analyze the kinetics of the initial reaction step in a wide range of the parameters. The region bounded by a multidimensional surface of the type $\varphi(P, T, \alpha, \ldots) = \mathbf{A}_0(P, T, \alpha, \ldots) - \mathbf{B}_0(P, T, \alpha, \ldots) = 0$, which is conventionally called the chain ignition region, actually defines the region where the system is capable of self-developing. The qualitative behavior of the system inside this region near the boundary is essentially related to the behavior of the functions $\mathbf{A}_0(P, T, \alpha, \ldots)$ and $\mathbf{B}_0(P, T, \alpha, \ldots)$ at the boundary. The boundary surface interrelates the critical values of the parameters, and, when some of them are fixed, the critical parameters can be quantitatively interrelated.

1. Chain Ignition Region for Methane in the T–α Plane

For constant pressure and reactor parameters, the expression $\mathbf{A}_0 - \mathbf{B}_0$ can be represented as the ratio of two polynomials of degree 5 with respect to α, with coefficients depending on T and P. Let us designate this ratio as $\varphi1(\alpha, T, P)$. The dependence of the critical parameters will then be determined by the constraint $\varphi1(\alpha, T, P) = 0$:

$$-\varphi1(\alpha, T) = K\alpha^5 + K_1\alpha^4 + K_2\alpha^3 + K_3\alpha^2 + K_4\alpha + K_5 - \alpha^2 P_0^2 a_1(C\alpha^2 + C_1\alpha + C_2) = 0. \quad (2)$$

The analysis of the pressure dependence of the coefficients in Eq. (2) shows that the positive terms tend to a limit as the pressure grows, whereas the negative terms increase infinitely with increasing pressure. It follows from this fact that Eq. (2) can have positive roots of the type $\alpha = \alpha(T)$ at sufficiently high P_0. The free term in this equation (K_5) is positive. Therefore, if this equation has positive roots, their number is even and does not exceed four. The existence of two roots means that at a given pressure the system has one critical temperature for two different compositions of the mixture. Then a function $T = T(\alpha)$ has at least one extreme point, at which the character of the dependence changes. The extreme points satisfy the equality $T'_\alpha = 0$; therefore, it follows from the equality $\varphi1'(\alpha, T) = (\partial\varphi1/\partial T)T'_\alpha + \partial\varphi1/\partial\alpha = 0$ that $\partial\varphi1/\partial\alpha = 0$. On the left-hand side of the last equation, we have a polynomial of degree 4 with respect to α for which $(\partial\varphi1/\partial\alpha)(0) > 0$. This polynomial must have an even number (at most four) of positive roots. However, this number is actually not larger than two, because, if there were four positive roots, the derivative $(\partial^2\varphi1/\partial\alpha^2)(0) > 0$ would have three positive roots, which is impossible, because the coefficient at α^3 is positive and, hence, one of the roots is necessarily negative. Thus, the curve $T = T(\alpha)$ has two extremes. Therefore, two solutions of Eq. (2) of the types $T = T(\alpha)$ and $\alpha = \alpha(T)$ correspond to each extreme. This implies that the domain of critical T and α values will be completely isolated if the other conditions are fixed. The regions in the T–α plane calculated by formula (2) are presented in Figs. 1a and 1b for the case of fixed pressure and reactor size and specified properties of the reactor wall. Figures 1a and 1b clearly demonstrate that the configuration of the resulting region is, in fact, a so-called "isol" divided by four turning points into regions with different types of $T(\alpha)$ and $\alpha(T)$ dependence. The calculations show that, when the ignition region is entered, the higher the critical temperature (T^*), the larger the deviation of $\mathbf{A}_0 - \mathbf{B}_0 > 0$ from zero. Therefore, T^* can be related to the reactivity that the system has after passing through the boundary of the ignition region. In particular, the dependence of the initial reactivity of the system on the mixture composition can be determined from the behavior of the $T(\alpha)$ function.

Lean and Rich Mixtures

The lower and upper isol boundaries and the left and right ones (Fig. 1) are divided by extreme points of the functions $T = T(\alpha)$ and $\alpha = \alpha(T)$, respectively, so that each has an ascending and a descending portion. Evidently, this division can provide an objective criterion for assigning an initial mixture to the "rich" or "lean" region. It is noteworthy that, as can be seen from Fig. 1b, the positions of the points demarcating these regions at opposite isol boundaries can vary with the factors changing the isol area in such a way that they drift toward each other as the isol area decreases and drift apart as it increases. At the lower pressure or reactor size limit, the isol is degenerated into a point representing $T \approx 850$ K and a nearly equimolar mixture. According to the data presented in Fig. 1a, the $T(\alpha)$ function in the region of rich mixtures decreases sharply (exponentially) with increasing α at the upper boundary and slowly at the lower boundary. For lean mixtures, on the contrary, this function increases rapidly at the upper temperature boundary and almost as rapidly at the lower boundary.

2. Chain Ignition Region for Methane in the P–T ($\alpha = \alpha_0$) Plane

It is clear from Fig. 1b that the isol area in the T–α plane decreases with decreasing pressure but most of the specific features of the isol configuration persist. Therefore, in the P–T space (at least, near 1 ± 0.5 atm), at vessel sizes within the limits set in the calculation of

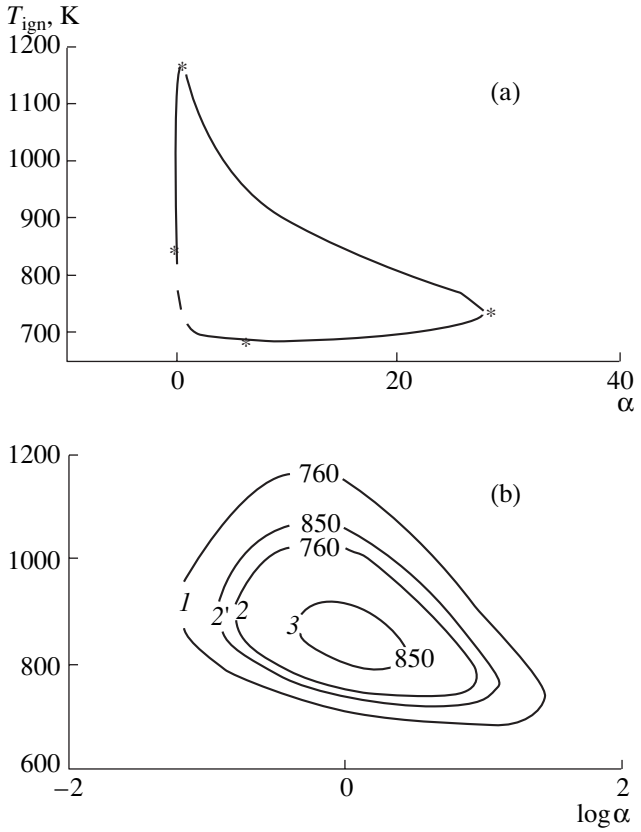

Fig. 1. T–α chain ignition region for methane: (a) in T–α coordinates at P_0 = 760 Torr and d = 3.6 cm and (b) in T– log α coordinates at P_0 = (*1*, *2*) 760 and (*2*', *3*) 850 Torr and d = (*1*) 3.6, (*2*, *2*') 2.5, and (*3*) 1.7 cm.

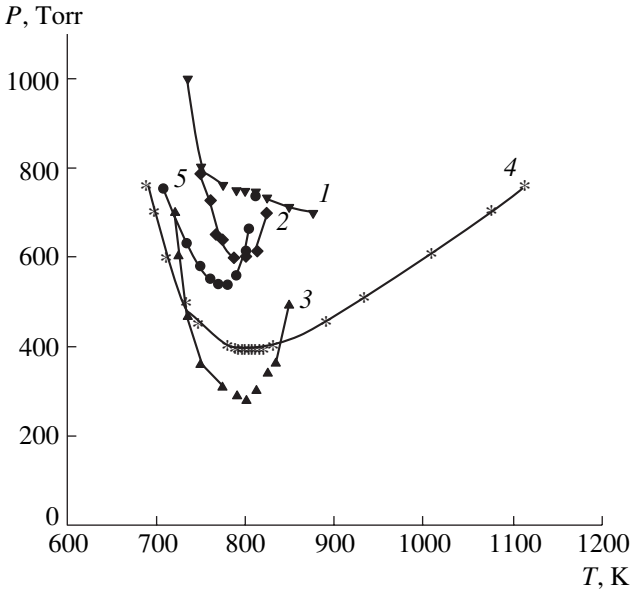

Fig. 2. Ignition regions in the P–T plane for $2CH_4 + O_2$ mixtures in a reactor with d = 3.6 cm: (*1*, *2*) data published [25] on the position of the hot and cold flash boundaries, respectively; (*3*) cold-flame boundary according to nonisothermic calculations [9]; (*4*) boundary of the chain ignition region calculated by formula (1); and (*5*) boundary of the cold-flame region calculated by formula (3) at $[R^\bullet] = [R^\bullet]_0 \times 500$.

the curves shown in Fig. 1b, we obtain a surface diverging up with respect to these parameters and converging down to the lower limit point. Cutting this surface with an (α_0–P) plane will give a U-shaped curve $P = P(T)$ U- or a C-shaped curve $T = T(P)$. The curve of the first type (Fig. 2, curve *4*) was obtained in this way for $\alpha_0 = 2$. Note that, at the pressures considered, such a mixture is considered (according to our classification) as rich at the upper temperature boundary and lean at the lower one. The nonmonotonic character of this curve can qualitatively be interpreted from the viewpoint presented in the previous section. Indeed, it is clear from Fig. 1b that the lower temperature boundary rises and the upper one falls with decreasing pressure. In view of the aforementioned role of T^*, this means that the relative reactivity of the system increases and decreases, respectively. In other words, for the left portion of curve *4* in Fig. 2, the minimum critical pressure corresponds to the highest reactivity state and, therefore, this branch as a whole corresponds to a process with a positive temperature factor of rate. For the right portion, this point corresponds to the minimum reactivity of the system, so that the slightest temperature increase at this pressure (and at all other pressure values in this branch) brings the system out of the ignition region. Thus, the lower limit point with respect to pressure divides curve *4* in Fig. 2 into the low- and high-temperature branches characterizing the positive and negative temperature effects (the latter referred to as the NTF of rate).

Interactions determining the configuration of the ignition region and the kinetic effects corresponding to different parts of the ignition region boundary can be revealed by estimating the main contributions to the $\mathbf{A}_0/\mathbf{B}_0$ as a function of temperature in the low- and high-value approximations and by selecting the major terms in α for lean and rich mixtures separately ($\alpha \ll 1$ and $\alpha \gg 1$, respectively).

Lower Temperature Boundary

Lean mixtures. $\mathbf{A}_0$ is determined by the ratio of a/L, and $\mathbf{B}_0$ is determined by the product sqa. Therefore, $\mathbf{A}_0/\mathbf{B}_0 \sim 1/sqL$, where only $L \sim 1/\alpha$ depends on α. Hence, $\mathbf{A}_0/\mathbf{B}_0 \sim \alpha\exp(-41\,500/RT)T^{1.4}$, and the critical temperature must decrease with increasing α to satisfy the condition $\mathbf{A}_0/\mathbf{B}_0 = 1$.

Rich mixtures. $\mathbf{A}_0 \sim al/m$, and $\mathbf{B}_0 \sim aqs$. Then $\mathbf{A}_0/\mathbf{B}_0$ is determined by the expression $l/mqs \sim 1/\alpha^2\exp(-77\,000)T^{-3.3}$ in view of $l \sim 1/\alpha$ and $q \sim \alpha$. The power function changes less rapidly with increasing temperature. Therefore, in the region considered, the $\mathbf{A}_0/\mathbf{B}_0$ is an increasing function of temperature and the critical temperature increases with increasing α.

Upper Temperature Boundary

At high temperatures, s and $m \sim 1$ and $1/L_1$ can be neglected.

Lean mixtures. In $\mathbf{A}_0$ the major term in α is $a/l \sim \alpha^2$, and the major term in $\mathbf{B}_0$ is qb, which is independent of α. Thus, we have $\mathbf{A}_0/\mathbf{B}_0 \sim a/lqb \sim \alpha^2\exp(+1400/RT)T^{-3.3}$. This dependence implies that the critical temperature increases with increasing α at rather high T values.

Rich mixtures. Here, a is almost independent of α, whereas $l \sim 1/\alpha$ and $q \sim \alpha$. Hence, $\mathbf{A}_0/\mathbf{B}_0 \sim al/bq \sim 1/\alpha^2\exp(+18300/RT)T^{-3.3}$. $\mathbf{A}_0/\mathbf{B}_0$ is a decreasing function of both temperature and α. As a consequence, the critical temperature decreases with increasing α.

These estimates agree with the data presented in Fig. 1, and the expressions from which we obtained the estimates elucidate the conditions under which the dynamic regimes in question occur.

Evidently, **at the lower temperature boundary**, the process is controlled by the decomposition of methyl hydroperoxide (reaction (V) in Table 1) and hydrogen peroxide (IX) and the chain propagation involving the $OH^{\cdot}$ and $CH_3O^{\cdot}$ radicals (reactions (VI) and (VII), respectively). Methane-deficient (lean) and oxygen-deficient (rich) systems experience difficulties in accumulation of an amount of peroxide CH_3OOH sufficient for decomposition. This is due to the fact that in both cases peroxide accumulation in the reaction between the $CH_3O_2^{\cdot}$ radical and methane (reaction (III)) is compensated by the consumption of the $CH_3O_2^{\cdot}$ radicals in the same reaction. $CH_3O_2^{\cdot}$ radical formation (reaction (I)) in lean mixtures is controlled by the lack of methyl radicals, whose concentration is limited by the amount of methane. In rich mixtures, it is oxygen-controlled. Therefore, the promotion of the process in lean mixtures is associated with the only reaction path involving oxygen, namely, the reaction sequence (VIII)–(IV)–(IX)–(VI), in which another branching peroxide (H_2O_2) forms readily and the fastest radical in the system ($OH^{\cdot}$) interacts with methane. In rich mixtures, deficient oxygen inhibits the accumulation of both methyl hydroperoxide and hydrogen peroxide in the above reaction sequence. Therefore, the process in this case can be promoted only by the activation of reactions whose rate increases more rapidly with temperature, namely, the decomposition of both peroxides and the interaction of the $CH_3O^{\cdot}$ radical with methane (reaction (VII)). The rate of the latter increases much more rapidly with temperature than the rate of the competitive reaction of the same radicals with oxygen (reaction (VIII)). This results in a strong inhibiting effect of oxygen in very rich mixtures.

At the upper temperature boundary, the region is restricted owing to the decrease in the number of branching events due to peroxide decomposition, although the decomposition itself does not control the process. In fact, this decrease is due to the activation of the inverse decomposition of the chain-leading $CH_3O_2^{\cdot}$ radicals (reaction (II)). When this reaction occurs efficiently, especially in oxygen-deficient (rich) mixtures, the interaction between methane and any radical results merely in accumulation of methyl radicals, which alone do not propagate the chain in the framework of the reaction network discussed. Naturally, addition of oxygen will compensate this effect until the competition between the chain-propagating interactions—the reactions of the $CH_3O^{\cdot}$ radical with oxygen (VIII) and methane (VII)—ends in favor of the former, in which this active radical is replaced by the less active radical $HO_2^{\cdot}$. Thus, the promoting effect of oxygen in rich mixtures opposes the inhibiting one in lean mixtures. Accordingly, methane inhibits the process in rich mixtures and promotes it in lean mixtures.

NONLINEAR CRITERION

Taking into account the nonlinear reactions, we can transform formula (1) into

$$\varphi = \mathbf{A} - \mathbf{B} = 0, \quad (3)$$

where

$$\mathbf{A} = a\left(\frac{2}{1+l} + \frac{(1+\delta_1)}{(1+1/l)} \times\left(\frac{2+(2+\gamma)/mL}{1+r+\gamma} + \frac{1}{L(1+1/(r+\gamma))}\right)\right),$$

$$\mathbf{B} = s(1+Q+Q_1)(1+\delta), \quad \delta = \frac{4k_{3'}[CH_3O_2^{\cdot}]}{k_{11}},$$

$$\delta_1 = \frac{2k_{19}[CH_2O^{\cdot}]}{k_{11}}, \quad Q_1 = f(1+a+b),$$

$$f = \frac{4k_{1'}[CH_3^{\cdot}]}{k_1[M][O_2]}, \quad \gamma = \frac{4k_{4'}[HO_2^{\cdot}]}{k_4[CH_4]}.$$

For such radical concentrations that the rates of linear decay and chain propagation involving these radicals are comparable with the recombination (negative chain interaction) and disproportionation (positive interaction) rates, formula (3) represents a modification of the linear criterion, with the contributions from nonlinear reactions added to the contributions from linear reactions of radicals of this type. In the case where the contributions δ, f, and γ from the recombination of the $CH_3O_2^{\cdot}$, $CH_3^{\cdot}$, and $HO_2^{\cdot}$ radicals, respectively, are added to the contributions from the decay of these radicals on the wall, they account for the enhancement of the inhibiting effect of these radicals. The space of parameters accessible to the reaction is thereby compressed. This compression in the P–T plane for α and

d = const from both the low- and high-temperature sides is illustrated by curve *5* in Fig. 2, which is obtained using formula (3) for $\alpha_0 = 2$, which corresponds to a rich mixture at the upper temperature boundary and to a lean mixture at the lower boundary. Here, taking into account the negative contributions from the quadratic interactions of the $CH_3O_2^{\cdot}$ (III') and $HO_2^{\cdot}$ (IV') radicals (δ in the formula for **B** and γ in the denominators of the expressions for **A**) gives a noticeable effect at the lower boundary, whereas the contribution f from the recombination of the $CH_3^{\cdot}$ radicals (I') brings about an effect at the upper boundary with an NTF. The positive contributions from the reactions of $CH_2O^{\cdot}$ and H_2O_2, which are active products of the same interactions (δ_1 and γ_1 in the numerators of the expressions for **A**), are responsible for the enhancement of the accelerating effect and extension of the reaction space. The same can be said about the seemingly positive interactions (XVIII) and (XX). The former indeed gives the chain-branching peroxide CH_3OOH; however, the decomposition of this peroxide is hampered at low temperatures. The latter propagates the chain and produces an accelerating effect owing to the fact that the active radical $CH_3O^{\cdot}$ is produced from the less active radical $CH_3O_2^{\cdot}$. However, this interaction competes with the formation of the major branching peroxide (reaction (III)) and plays a negative role toward this peroxide. Therefore, the contributions from nearly all of the nonlinear reactions mentioned exert an effect on both **A** and **B**. This effect may vary from one region of parameters to another. Therefore, the size and configuration of the region of parameters where the system is capable of self-developing change considerably during the reaction.

Cold Flames

The data on the linear reactions (see Table 2) show that the formation of stable products in these reactions is accompanied by a considerable heat release and can change the state of the system relative to the initial state even at very low conversions. In other words, a process starting at low temperatures can move the system to the high-temperature region owing to the exothermic recombination of the slowly reacting radicals $CH_3O_2^{\cdot}$. This enhances peroxide decomposition to accelerate the process but also enhances the inverse decomposition of the $CH_3O_2^{\cdot}$ radical to oxygen and $CH_3^{\cdot}$. The latter is accumulated and recombines to release a great amount of heat upon the formation of new products and shifts the upper boundary toward low temperatures. In our opinion, this process can manifest itself as a short-term flash with a sharp quenching edge due to the system leaving the ignition region. Thus, curve *5* in Fig. 2 is a boundary of the cold-flame region (when calculating it by formula (3), we additionally took into account the negative contributions from reactions (XVIII) and (XX)). Figure 2 makes it possible to see which of the calculated boundaries of the cold-flame region is closest to the boundary experimentally found in [25] (curve *2*). Figure 2 also shows how the system gets into the cold-flame region owing to the exothermic nonlinear processes and, possibly, leaves it because of "collision" with the upper temperature boundary characterized by an NTF. The upper temperature boundary shifts toward low temperatures, again due to the nonlinear reactions.

Kinetics at an Elevated Pressure

The role of nonlinear reactions even at the lowest degrees of burnout shows itself as a fast transition from the initial autoacceleration to a quasi-steady-state regime (so-called slow oxidation). Researchers treat this process as a delay of the active process (against the background of which one- and (or) two-step cold and then hot flashes can occur). The probability of phenomena similar to cold flashes decreases with increasing pressure increase (at $P \gg \sim 1$ atm and the other conditions being fixed) due to the decrease in the probability of the inverse decomposition of chemically activated methylperoxy radicals. Indeed, these radicals are better stabilized in collisions but still can decompose if a temperature sufficient for this decomposition is achieved due to nonlinear processes. If this decomposition does not occur, then the system can get into a hot flash region immediately after the slow oxidation step resulting in heating of the system and acceleration of the process. As for the peroxy radicals, the activation of peroxide decomposition, which is not controlled by collisions, becomes independent of the pressure at very high pressure values but depends on the temperature. The role of linear decay of radicals becomes insignificant compared to that of the nonlinear decay.

Analyzing the influence of the aforementioned changes on criterion (3) in the case of high pressures, note that the configuration of the ignition region in the T–α plane remains qualitatively unchanged.

The results of the calculation of the **A/B** criterion under conditions close to those in Melvin's experiments [22] on ignition delays for rich methane–air mixtures at high pressures (~40–150 atm) and low initial temperatures (620–750 K) are shown in Fig. 3. Recall that a characteristic two-step process was observed [22], in which the ignition delay τ was determined as the time elapsed from the instant the reactants are let in to the instant the slow temperature increase is replaced by an autoaccelerated one.

In this work, when simulating the Melvin delays, we use a nonlinear reaction network similar to that described in [17], which is based on the irreversible formation of peroxy radicals at high pressures and low

temperatures, but taking into account the recombination of methyl radicals (of the linear reactions, this network includes peroxide formation, decomposition, and decay). Compare Melvin's experimental data, according to which the order with respect to oxygen for the slow step is –0.6, with the data presented in Figs. 1 and 3. As is mentioned above, the behavior of the system at the lower and, perhaps, upper temperature boundaries at low and high pressures is qualitatively similar: oxygen acts as an inhibitor and a promoter, respectively. This suggests that the behaviors of the rich mixtures established experimentally for these conditions and those predicted by our analysis and calculations coincide satisfactorily. The delay is interpreted as a process beginning at the lower temperature boundary, and the second step is the continuation of the same process upon a considerable heating favoring the achievement of the upper boundary. Note that, during the delay, **A/B**, plotted in Fig. 3, is determined mainly by the quadratic contributions from the interactions of methyl and hydroperoxy radicals, while, during oxygen combustion and the second step, it is determined by the nonlinear contributions from interactions of a higher degree with respect to the concentration of radicals, especially methyl radicals.

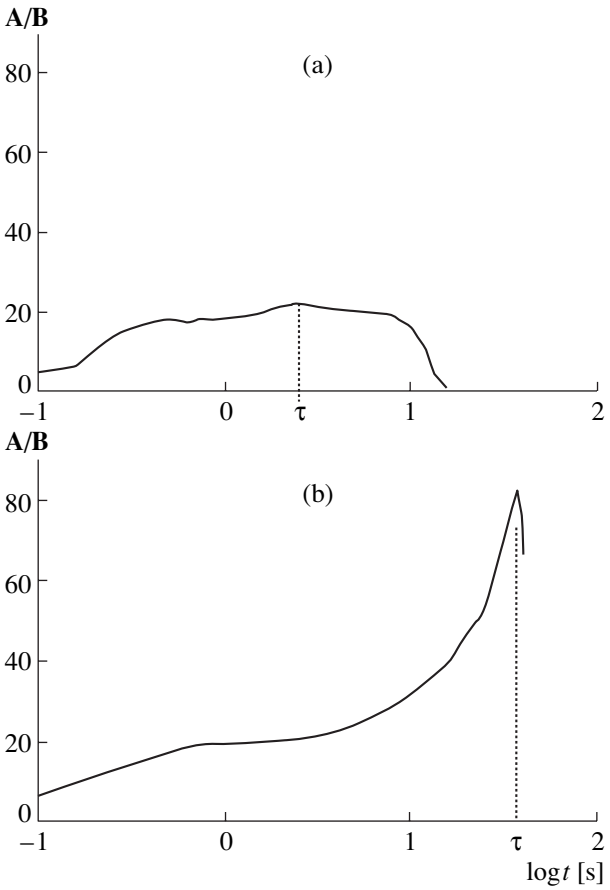

Fig. 3. Simulation of the Melvin delay by the direct calculation of the dynamic criterion **A/B** for methane–air mixtures of composition (a) 0.9 : 0.1 and (b) 0.6 : 0.4, $P_0 \sim$ 100 atm, $T_0 \sim 700$ K, and $d = 2.5$ cm; τ is the delay time for the second step.

RESULTS AND DISCUSSION

Note that experimental studies of methane oxidation in a range of conditions as wide as in the present work are rarely reported in the literature. For example, most of the earlier attempts to study the kinetics of this system in a relatively wide range of initial mixture compositions were restricted to problems on so-called normal flame distribution in rather lean mixtures according to the standard classification ($\alpha \le 0.5$), which were studied in narrow pipes. Among those work, note the study in which the reaction order with respect to methane was observed to decrease from $n = +0.65$ to $n = -0.5$ as the initial temperature was raised from 700 to 1000°C in pipes with a diameter of 0.1–0.5 cm [28]. Although the reaction rate measured in that work (in terms of CO accumulation) is likely to be close to the maximum rather than the initial rate, the effect observed is undoubtedly similar to the effect illustrated in Fig. 1. When the data in Fig. 1b are extrapolated to the experimental conditions as in [28] (that is, small reactor sizes and accordingly high total pressures), it turns out that the mixtures examined in that work fall into the region of rich mixtures at the upper temperature boundary. Later there was a study of the kinetics of methane oxidation at a varied composition parameter $\alpha = 1S$–$4S$ (S is the stoichiometric composition) in the presence of nitrogen at 800–1200 K under static conditions [29]. That study and our calculations provided very similar data as to the decrease in the reaction order with respect to methane on going from the lower to the upper boundary owing to the similarity of the initial parameters of the system (in the experiments $P \approx$ 100–500 Torr and $d = 3$ cm). It is shown [29] that the methane-inhibited oxidation is characterized by a high selectivity toward unsaturated products, whose source is ethane, the product of the recombination of $CH_3^{\cdot}$ radicals. This was confirmed [30] by numerical simulation of the kinetics inside the ignition region. Note that our data, which readily explain this phenomenon, were obtained using a reaction network simpler than that suggested in [29, 30] for the simulation of ethane and ethylene formation. An alternative reaction $CH_3^{\cdot} + O_2 \longrightarrow CH_2O + HO^{\cdot}$, whose addition to our network does not qualitatively change the conclusions as to the behavior of the system in the rich mixture region, was taken into account in [30] along with the formation of the $CH_3O_2^{\cdot}$ radical by reaction (I).

The qualitative dependence suggested for the ignition region boundary ($T(\alpha)$ for the rich and lean mixtures at the high- and low-temperature limits can be used to estimate the apparent activation energy of methane oxidation. Our estimate for the rich mixtures at the upper tem-

perature boundary, $E_{app} \sim -18$ kcal/mol, is close, for example, to Neuman's value $E_{app} \sim -14$ kcal/mol for the reaction controlling the oxidation of RH hydrocarbons under conditions of substantial reversibility of the $RO_2^{\cdot}$ formation reactions of the type (I)–(II) [2] (that is, at cold-flame temperatures in the NTF branch). It was also inferred [9, 27] that the decrease in the $CH_3O_2^{\cdot}$ concentration caused by an increasing temperature affects the cold-flame mechanism in methane combustion and that the recombination of the $CH_3^{\cdot}$ radicals should necessarily be taken into account. These conclusions differ from those following from our analysis only in the interpretation of the role of the NTF phenomenon itself in this mechanism. Indeed, the authors of earlier works [9, 27] did not ascertain whether NTF brings about cold flame or causes accompanying phenomena. It follows from our analysis that the effect of NTF is directly related to the activation of the linear inverse decomposition of methylperoxy radicals at rather high temperatures and, hence, it is responsible only for the decrease in the reaction rate (quenching) in the corresponding region of the initial parameters. The nonlinear effects play the main role in both the initial stationary heating and the resulting autoacceleration: the cold flame is quenched at temperatures much lower than follow from the position of the NTF boundary in the linear approximation. Curve *4* in Fig. 2, with an NTF branch, which is calculated by formula (1) for $\alpha = 2$, is qualitatively similar to the characteristic U-shaped boundary of the cold-flame regions found experimentally [25] and numerically [9] (Fig. 2, curves *2*, *3*, respectively). It should be noted that, as compared to curve *3*, curve *4* is closer in pressure to the region behind curve *2* [25]; however, its NTF branch is smoother than those of curves *2* and *3*. All these data imply that the simple linear model we propose describes the system near the boundaries qualitatively better than the large network with nonlinear reactions used in [2]. The nonlinear network (also reduced much) qualitatively correctly reflects the specific features of the movement of the system from the lower temperature boundary to the upper one and the movement of the upper boundary toward low temperatures during the process. Perhaps, the agreement with the published data [25] would be better if the linear and nonlinear decay reactions involving the $OH^{\cdot}$ and $CH_3O^{\cdot}$ radicals were taken into account.

Note that the model, which is far from completion and ignores isothermicity, demonstrates, in Fig. 3, all the characteristic features of the behavior of the system at high pressures. These features were noted in [22] and refer to both the first and second steps. Even the upper temperature limit appears similarly in the experiments and calculation: it shows itself as a sharp decrease in **A**/**B** and the ΔT signal at the end of the second step. Of course, the ultimate heating in the second step in the experiment far exceeds the upper temperature boundary in Fig. 1 and is determined by the nonlinear reactions of radicals and by the transformations of their products accompanied by the formation of energy-consuming products. Melvin [22] insisted on the key role of the reactions involving molecular and atomic hydrogen in the oxidation mechanism. From the results of the present work, we can make the following conclusion as to the thermal stage of the reaction under various conditions, not only at high pressures: the reaction of hydrogen with oxygen can make an important contribution to the ultimate heating in this step, but it is not the cause of this step.

CONCLUSIONS

The conclusions as to the dynamics of the process drawn from the behavior of the system near the boundaries of the ignition region are qualitative and are not claimed to cover all situations of interest. In particular, a deeper understanding of the behavior of the system inside the ignition region can be achieved by nonisothermic simulation of the kinetics like that in [26], where the nature and conditions of the thermal explosion of hydrogen–oxygen mixtures inside the ignition peninsula were studied.

The specific features of methane oxidation at high temperatures and low pressures are beyond the scope of this article. The mechanism of this process, as compared to the mechanism considered here, will additionally include hydrogen formation and oxidation steps. In this case, the nonlinear effects related to the reactions on the wall should be taken into account [6]. The criterion suggested implicitly takes into account the influence of diluents, for example, water. However, water acts not only as an efficient collision agent, particularly at high temperatures. This issue also requires a special study, which is expected to be very important for solving a variety of practical problems.

APPENDIX

I. Expressions for Constants Depending on Pressure and Mixture Composition

A. Linear decay of radicals. The rate constants of radical decay on the vessel wall are classified according to the degree of accommodation to the wall into diffusion ones (for the radicals $CH_3^{\cdot}$ (reaction (XIII)), $HO_2^{\cdot}$ (XII), and $CH_3O_2^{\cdot}$ (XI)) and combined ones (for the peroxides H_2O_2 (X) and CH_3OOH (XIV)). The diffusion constants depend on the pressure (P, Torr): $k_{diff} = (ZD)/P$, where $Z = 4\pi^2/d^2 760(T/273)^{1.6}$, d is the vessel diameter, and D is the pressure-independent diffusion coefficient ($D_1 = 0.135$ for $CH_3O_2^{\cdot}$ and CH_3O_2H, $D_2 = 0.198$ for $HO_2^{\cdot}$ and H_2O_2, and $D_3 = 0.347$ for $CH_3^{\cdot}$), or

$$k_{diff} = \frac{ZD}{P} = 2.9 \times 10^4 \frac{D(T/273)^{1.6}}{Pd^2}. \quad \text{(i)}$$

Table 3. Parameters of the association and decomposition reactions with the participation of the active centers involved in formula (*ii*) [18]

N*	$k^0 = A^0T^n \exp(-E^0/RT)$			$k^\infty = A^\infty T^n \exp(-E^\infty/RT)$			$F = f_1T^{n_1}\exp(-Tm_1) + f_2T^{n_2}\exp(-Tm_2)$					
	A^0	E^0	n	A^∞	E^∞	n	m_1	m_2	f_1	f_2	n_1	n_2
(I)	0.58×10^{26}	0	–3.3	0.78×10^9	0	1.2	0	0	0.446	-0.13×10^{-3}	0	1
(V)	0.6×10^{18}	39.8	0	0.60×10^{15}	42.3	–	0	–	0	0	0	0
(IX)	0.12×10^{18}	45.5	0	0.30×10^{15}	48.5	–	0	–	0.5	0	0	0
(I')	0.13×10^{42}	2.76	–7	0.36×10^{14}	0	–	0.014	8.5×10^{-4}	0.385	0.620	0	0

* The reactions are numbered as in Tables 1 and 2.

Combined constants are introduced for peroxides with a low accommodation to the reactor wall, due to which their decay is mainly controlled by surface kinetics. The relationship between the kinetic constant and the accommodation coefficient of a species is given by the formula $\eta = \frac{k_{\text{kin}}d}{v}$, where v is the mean velocity of the species. Taking into account that $\eta_{CH_3O_2H} = 0.67 \times 10^{-5}$ and $\eta_{H_2O_2} = 0.23 \times 10^{-5}$ for k_{kin} at 728 K and d = 7 cm [7], we obtain $k_{\text{kin}(CH_3O_2H)} \approx 0.0125T^{0.5}/d$ and $k_{\text{kin}(H_2O_2)} \approx 0.005T^{0.5}/d$. Since $\frac{1}{k_{\text{komb}}} = \frac{1}{k_{\text{diff}}} + \frac{1}{k_{\text{kin}}}$, the decay of peroxides also begins to depend on diffusion as the pressure is raised.

B. Association and decomposition reactions. The rate constants for the recombination of $CH_3^\cdot$ radicals (I') and for the reaction between a $CH_3^\cdot$ radical and an oxygen molecule (I) and the decomposition rate constants for the peroxides CH_3O_2H (V) and H_2O_2 (IX) depend on the pressure according to the formula

$$k = \frac{k^0[\text{M}]k^\infty}{k^0[\text{M}] + k^\infty}F, \qquad \text{(ii)}$$

where k^0 and k^∞ are the constants at the low- and high-pressure limits, respectively; [M] (mol/cm^3) = PN is the total concentration of all components in the gas mixture at a pressure P (Torr) and $N = 0.59 \times 10^{-7}$ (273/T); and $F = F(T)$ is the so-called distribution function of intermediate complexes.

Only k^0 values are presented in Tables 1 and 2, while Table 3 lists all values appearing in formula (ii) [18].

The rate constant of the inverse decomposition of the $CH_3O_2^\cdot$ radical (II) also depends on the pressure and is calculated using the equilibrium constant $K_{1,2} = R_{\text{eq}}T\exp((\Delta H^0_{298}/RT) - \Delta S^0_{298}/R)$ by the formula $k_2 = k_1/K_{1,2}$, where R_{eq} = 82 cm^3 atm mol^{-1} K^{-1}, ΔH^0_{298} = –32.3 kcal/mol, ΔS^0_{298} = –31.05 cal mol^{-1} K^{-1} [19], and the concentrations of the reactants are expressed in cm^3/mol.

C. Concentrations expressed in terms of component fractions and ratios. In general, the factor 1 at [M] in formula (ii) can be written as the sum of the fractions of the components in the mixture of $[O_2]_0$, $[CH_4]_0$, and $[N_2]_0$. Taking into account the relative effectiveness of these components in the activation and deactivation of active complexes gives [M] = $PN(0.8[O_2]_0 + 1.7[CH_4]_0 + [N_2]_0)$. The concentration of the components is expressed in terms of their pressures and fractions in the mixture, for example, $[CH_4] = [CH_4]_0PN$. The fractions of the components are most frequently expressed in terms of the ratios α and β defined as $1 = [O_2]_0 + [CH_4]_0 + [N_2]_0 = [O_2]_0(1 + \alpha + \beta)$. For diluent-free mixtures, the terms involving concentration in formulas (1)–(3) are written in terms of α as

$$a = \frac{a_1\alpha}{(1+\alpha)}, \quad a_1 = \frac{k_3PN}{k_{11}}, \quad q = q_1(1+\alpha),$$

$$q_1 = \frac{k_{13}}{k_1[\text{M}]PN}, \quad r = 1 + \frac{r_1\alpha}{(1+\alpha)}, \quad r_1 = \frac{k_{12}}{k_4PN}.$$

II. Radical Concentrations

The initial concentrations of the radicals $HO_2^\cdot$, $CH_3^\cdot$, and $CH_3O_2^\cdot$ were estimated from the quasi-steady-state relationships for the rates of chain initiation (0) and of the propagation and decay reactions (linear with respect to radicals):

$$[HO_2^\cdot]_0 \approx ((k_0/k_4)\exp((E_4 - E_0)/RT)[O_2])/r, \qquad \text{(iii)}$$

$$[CH_3^\cdot]_0 \approx (k_0/k_1)\exp(-E_0/RT)T^{3.3}[CH_4]/(1+q), \qquad \text{(iv)}$$

where $q = k_{13}/(k_1T^{-3.3}[O_2])$.

The expression for $[CH_3O_2^\cdot]$ was derived using formula (iv) for $[CH_3^\cdot]$:

$$[CH_3O_2^{\cdot}]_0 = (k_0/k_{11})\exp(-E_0/RT)[O_2] \times [CH_4]/(1 + (1 + q)(1 + a + b)). \quad (v)$$

ACKNOWLEDGMENTS

We thank V.V. Azatyan, corresponding member of the Russian Academy of Sciences, for helpful discussion.

REFERENCES

1. Lewis, B. and von Elbe, G., *Combustion, Flames, and Explosions of Gases*, New York: Academic, 1961.
2. Shtern, V.Ya., *Mekhanizm okisleniya uglevodorodov v gazovoi faze* (Mechanism of Hydrocarbon Oxidation in the Gas Phase), Moscow: Akad. Nauk SSSR, 1960.
3. Semenov, N.N., *O nekotorykh problemakh khimicheskoi kinetiki i reaktsionnoi sposobnosti* (Problems of Chemical Kinetics and Reactivity), Moscow: Akad. Nauk SSSR, 1954.
4. *Khimicheskaya kinetika i tsepnye reaktsii* (Chemical Kinetics and Chain Reactions), Moscow: Nauka, 1966.
5. *Tsepnye reaktsii* (Chain Recations), Moscow: Nauka, 1981.
6. Azatyan, V.V., *Arm. Khim. Zh.*, 1988, vol. 41, p. 7.
7. Vedeneev, V.I., Karnaukh, A.A., Mantashyan, A.A., and Teitel'boim, M.A., *Kinet. Katal.*, 1990, vol. 31, no. 1, p. 98.
8. Mantashyan, A.A. and Sarkisyan, L.A., *Khim. Fiz.*, 2000, vol. 19, no. 2, p. 115.
9. Sokolov, O.V., Parfenov, Yu.V., Arutyunov, V.S., Basevich, V.Ya., and Vedeneev, V.I., *Izv. Akad. Nauk, Ser. Khim.*, 1996, vol. 10, p. 2445.
10. Ivanova, A.N. and Tarnopol'skii, B.L., *Kinet. Katal.*, 1979, vol. 20, no. 6, p. 1541.
11. Ivanova, A.N., Tarnopol'skii, B.L., and Karnaukh, A.A., *Kinet. Katal.*, 1997, vol. 38, p. 485.
12. Andrianova, Z.S., Ivanova, A.N., and Azatyan, V.V., *Khim. Fiz.*, 1998, vol. 17, p. 91.
13. Karnaukh, A.A., Ivanova, A.N., Tarnopolskii, B.L., and Andrianova, Z.S., *5th Int. Congress on Toxic Combustion Byproducts*, Dayton: Ohio Univ., 1997, p. 77.
14. Ivanova, A.N. and Karnaukh, A.A., *XII Simpozium po goreniyu i vzryvu* (XII Symp. on Combustion and Explosion), Chernogolovka, 2000, part 2, p. 65.
15. Karnaukh, A.A. and Ivanova, A.N., *Combustion and Atmospheric Pollution*, Frolov, S.M. and Starik, A.M., Eds., Moscow: TORUS-PRESS, 2003, p. 67.
16. Ivanova, A.N., Karnaukh, A.A., and Barkalov, I.M., *Tezisy CTAF-97* (Proc. CTAF-97), St. Petersburg, 1997, p. 47.
17. Vedeneev, V.I., Gol'denberg, M.Ya., Gorban', N.I., Karnaukh, A.A., and Teitel'boim, M.A., *Kinet. Katal.*, 1988, vol. 29, p. 1297.
18. Baulch, D.L., Cobos, C.J., Cox, R.A., *et al.*, *Combust. Flame*, 1994, vol. 98, p. 59.
19. Slagle, I.R. and Gutman, D., *J. Am. Chem. Soc.*, 1985, vol. 107, p. 5342.
20. Liu, A., Mulac, W.A., and Jonah, C.D., *Int. J. Chem. Kinet.*, 1987, vol. 19, p. 25.
21. Vedeneev, V.I., Gol'denberg, M.Ya., and Teitel'boim, M.A., *Khim. Fiz.*, 1986, vol. 5, p. 1106.
22. Melvin, A., *Combust. Flame*, 1966, vol. 10, p. 120.
23. Karnaukh, A.A., Kuzina, S.I., and Mikhailov, A.I., *6 mezhdunarodnaya konferentsiya po molekulyarnoi biologii, khimii i fizike neravnovesnykh sistem* (6th Int. Conf. on the Molecular Biology, Chemistry, and Physics of Nonequilibrium Systems), Ivanovo, 2002, p. 50.
24. Benson, S.W. and Nangia, P.S., *Acc. Chem. Res.*, 1979, vol. 12, no. 7, p. 223.
25. Vanpee, M., *C. R. Acad. Sci.*, 1956, vol. 243, p. 8041.
26. Andrianova, Z.S., Ivanova, A.N., and Azatyan, V.V., *Kinet. Katal.*, 2002, vol. 43, p. 182.
27. Vedeneev, V.I., Arutyunov, V.S., Basevich, V.Ya., Parfenov, Yu.V., and Bernatosyan, S.G., *Khim. Fiz.*, 2000, vol. 19, no. 4, p. 94.
28. Kozlov, G.E., *Proc. Seventh Symp. on Combustion*, Pittsburgh, 1957, p. 142.
29. Cathonnet, M. and James, H., *J. Chem. Phys.*, 1975, vol. 72, no. 2, pp. 247, 253.
30. Andrianova, Z.S., Ivanova, A.N., Matkovskii, P.E., and Startseva, G.P., *Kinet. Katal.*, 1993, vol. 34, no. 3, p. 396.